Continuous wave monolithic quasi-phase-matched optical parametric oscillator in periodically poled lithium niobate

C. R. Phillips,* J. S. Pelc, and M. M. Fejer

E. L. Ginzton Laboratory, Stanford University, 348 Via Pueblo Mall, Stanford, California 94305, USA
**Corresponding author: chris.phillips@stanford.edu*

Received May 10, 2011; revised July 1, 2011; accepted July 3, 2011;
posted July 5, 2011 (Doc. ID 147308); published August 1, 2011

We demonstrate a monolithic and quasi-phasematched singly resonant cw optical parametric oscillator in periodically poled lithium niobate. The threshold is 1.0 W and the OPO delivers up to 0.98 W signal power tunable between 1750 and 1950 nm (2710 and 2340 nm idler, respectively). We identify cascaded parasitic oscillation effects and analyze their behavior theoretically, showing good agreement with our experiment. The analysis of parasitic effects points the way to improved device designs that should enable stable, compact, and frequency-tunable sources.

OCIS codes: 190.4970, 190.4360.

Optical parametric oscillators (OPOs) provide a means to extend the spectral coverage of mature laser sources. Since the first demonstration of a cw singly resonant OPOs [1], the advent of quasi-phasematching (QPM) and periodically poled lithium niobate (PPLN) has enabled highly efficient devices with low thresholds for oscillation [2]. However, the construction and operation of OPOs can be quite complex; reducing this complexity would enable a more widespread deployment of cw OPOs.

In this Letter, we report on a monolithic congruent PPLN OPO, where the path of the resonant signal wave is entirely within the PPLN QPM grating [3]. This approach has several advantages, including mechanical and thermal stability, simplicity of operation and alignment, and the possibility of low losses since the monolithic resonator has no lossy internal interfaces, and, importantly for mid-IR operation, has no (possibly absorptive) air path. This monolithic configuration was accomplished by applying an angled spherical polish and a highly reflective (HR) coating to two of the facets of the PPLN crystal and using total internal reflection on one side of the crystal to form a closed resonant path [3], see Fig. 1. To ensure that the resonator axis was within the 1 mm thick crystal aperture, the angles of each curved facet were tested optically during the OPO fabrication process via a reflection measurement with a HeNe laser.

In our OPO, the mirror curvature is $R = 40$ mm, and the crystal has dimensions $52 \times 5 \times 1$ mm. The PPLN crystals were fabricated by Crystal Technology, Inc. and have a QPM period of $\Lambda_G = 30.9\,\mu$m. We resonate the short-wave signal, which is tuned around $1.8\,\mu$m. The coating for the curved input crystal facet is HR between 1.7 and $2.0\,\mu$m (reflectance $R > 99.9\%$), highly transmissive between 2.4 and $2.9\,\mu$m ($R < 5\%$), and has $R \approx 5\%$ at $1.064\,\mu$m. The coating for the output facet has $R \approx 99.5\%$ between 1.7 and $1.9\,\mu$m, $R < 5\%$ between 2.4 and $2.9\,\mu$m, and $R \approx 5\%$ at $1.064\,\mu$m. The focusing parameter is defined as $\xi_j = L/(k_j w_{j0}^2)$ $(j = i,\ s,\ p)$, where L is the QPM grating length, $k_j = 2\pi n_j/\lambda_j$ is the wave vector at wavelength λ_j, and w_{j0} is the $1/e^2$ intensity radius of wave j at the beam waist. We focused the pump to slightly looser than confocal ($\xi_p \approx 0.9$), while the cold-cavity mode defined by the geometry of the PPLN crystal is focused slightly tighter than confocal ($\xi_s \approx 1.3$),

In earlier experiments using MgO:PPLN monolithic OPO samples, only part of the resonant mode's path was within the QPM grating. We observed in that case a spoiling of the modes of the cavity over time scales of several minutes while the OPO oscillated, eventually bringing the OPO below threshold. We attribute this effect to a combination of parasitic green light generation in the QPM grating [4], with subsequent pyroelectric effects in the unpoled region that are usually suppressed by the QPM grating [5]. To achieve long-term OPO operation, we ensured that the signal mode propagated entirely within the QPM grating, as illustrated in Fig. 1.

For all measurements of the OPO performance, the cavity was aligned such that the threshold pump power was minimized, with a 1.0 W threshold. We measured the output signal power as a function of the pump power, as shown in Fig. 2(a). At a pump power P_p of 7.0 W, we observed an output power of 0.98 W in the signal spectral region, with pump depletion of approximately 80% (corresponding to an idler power of 2.3 W from the quantum defect). Given the 0.5% output-facet transmission, this output power and pump depletion are consistent with round-trip signal losses of 1.57% (which in turn are consistent with ≈0.1 %/cm propagation losses). From OPO theory [2], assuming that $d_{33} = 27$ pm/V, the cavity losses required to reach a 1.0 W threshold are 1.65%, in good agreement with the above loss estimate.

For bulk OPOs with near-confocal focusing ($\xi_s \approx 1$ and $\xi_p \approx 1$) high pump depletion can be achieved at $N \approx 2.5$,

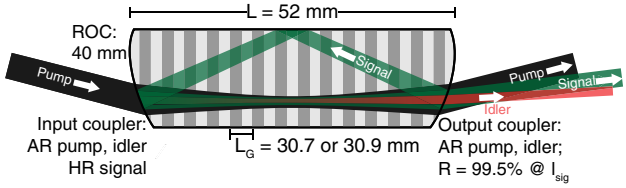

Fig. 1. (Color online) Schematic of the OPO, showing the path of the resonant signal.

with behavior comparable to plane-wave OPOs [2,6], where the times above oscillation threshold is defined as $N = P_p/P_{\text{th}}$. Based on our estimate of the absorption losses, the available pump power of 8 W, and 90% pump depletion, an output coupler of around 4% would lead to optimal signal output power of approximately 3.4 W.

Next, we studied the spectral properties of the OPO by coupling the output signal wave into a single-mode fiber and routing the light to a Michelson interferometer-based wavemeter and spectrum analyzer. We measured the oscillating signal wavelength as a function of the crystal temperature, the results of which are shown as squares in Fig. 2(b). We operated the OPO between 135° and 200 °C to avoid photorefractive effects at low temperature and damage to the coatings at high temperatures. The solid curve in Fig. 2(b) is a fit to the temperature-dependent Sellmeier equation for congruent $LiNbO_3$ [7], showing good agreement with the data. The fit includes a 3 °C temperature offset, which could be due to a miscalibration of the temperature sensor, slight beam noncollinearities, or self-heating from absorbed signal power. As a typical result, the measured FWHM of the signal spectrum at 166 °C was 0.04 nm (3.66 GHz), which is at the resolution limit of our wavemeter. This value is approximately 2.7-times the free spectral range of the OPO cavity (1.34 GHz).

While operating the OPO, we observed several additional effects that caused changes to the signal power and its spectrum. To characterize these effects we used an acousto-optic modulator to pulse the pump. In this way, effects that develop over different characteristic time scales could be isolated (thermal, photorefractive, cavity-loss, etc.). The thermal time-scale t_{therm} (the time taken for a temperature profile to develop across the signal beam due to absorption of the signal) is approximately 1 ms in our case. We therefore generated pump pulses with a duration of $t_{\text{pulse}} = 50\,\mu\text{s}$, so that $t_{\text{pulse}} \ll t_{\text{therm}}$. The relatively high signal absorption of

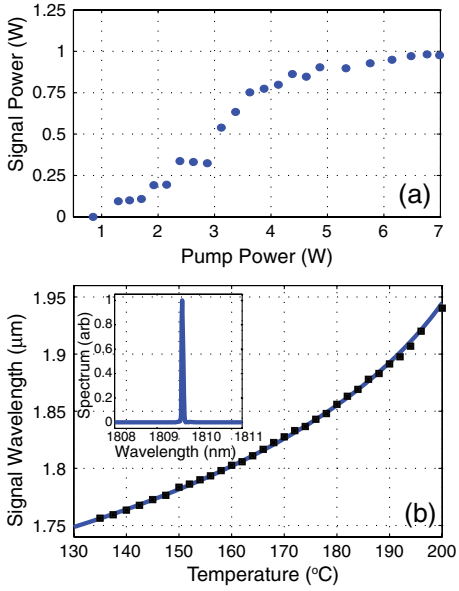

Fig. 2. (Color online) (a) Output signal power as a function of input pump power, (b) signal wavelength tuning with temperature. Inset: spectrum, measured with 0.04 nm resolution.

$0.1\,\%/\text{cm}^{-1}$ caused a significant thermal lens when operating with a cw pump. Therefore, a low duty cycle of 5% was used for these pulsed-pump measurements in order to keep the total thermal load of the cavity small. The pulsed-OPO signal output was sent into a spectrometer; spectral content below 1.7 μm was filtered with a Ge window. A corresponding oscilloscope trace of OPO output powers is shown in Fig. 3.

When operating at 130 °C (1.748 μm signal), we observed a strong additional "cascaded" signal at 1.762 μm when $N > 2$. This wavelength corresponds to a frequency shift $\delta f \approx 1.37$ THz; inspection of the dispersion of $LiNbO_3$ shows that a backward-propagating THz wave at this frequency is quasi-phasematched [7,8], so the presence of this wavelength corresponds to optical parametric amplification with a THz idler wave (THz-OPA). At 150 °C (1.780 μm) we observed signals at 1.795 μm ($\delta f \approx 1.37$ THz), 1.864 μm ($\delta f \approx 7.4$ THz), and 2.005 μm ($\delta f \approx 18.76$ THz); the frequencies of these additional processes are close to strong peaks in the e-wave Raman spectrum of $LiNbO_3$ [9], and hence we attribute them to stimulated Raman scattering (SRS). Figure 3 shows the reflected and transmitted pump, the transmitted signal, and the transmitted Stokes wave when operating at 150 °C. Cascaded-signal waves have been observed in other cw OPOs [8,10–12]; the gain for these waves should be quantified in order to ensure single-mode operation.

To quantify these cascaded processes, note that the gain mechanism relies on an essentially nonpropagating wave (molecular vibrations for SRS, and a strongly absorbed THz wave for THz-OPA). By assuming a gain proportional to the signal intensity, that both the OPO signal and cascaded-signal beams are Gaussian modes of the low-loss cavity, and then performing modal overlap integrals [13], it can be shown that the round-trip gain for the cascaded-signal beam is given by

$$G \approx \left(\frac{g}{I_{s1}}\right)\left(\frac{1}{k_{s1}} + \frac{1}{k_{s2}}\right)^{-1} \frac{\phi_{\text{Gouy}}}{\pi} P_{s1}, \tag{1}$$

where subscripts $s1$ and $s2$ denote the OPO signal and cascaded-signal waves, respectively, g/I_{s1} is the gain coefficient at the cascaded-signal wavelength, and ϕ_{Gouy} is the Gouy phase accumulated from diffraction in the

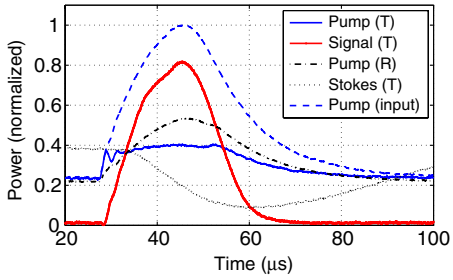

Fig. 3. (Color online) Pulsed-OPO measurement at peak $N \approx 2.5$ and 150 °C. Powers are shown for the transmitted and reflected pump (solid blue and dot-dashed black), the transmitted signal (solid red), the transmitted Stokes (dotted black), and the input pump (dashed blue). The signal and Stokes wavelengths are 1.78 and 2.005 μm, respectively. The powers are rescaled for clarity; the Stokes wave was measured on a slow pyroelectric detector.

region of the cavity where cascaded-signal gain occurs. The Gouy phase emerges from integrating $1/w_s(z)^2$ over the cavity, where $w_s(z)$ is the signal $1/e^2$ beam radius.

Any generated THz wave components diffract and are absorbed rapidly. Suppose that THz diffraction can be neglected, which is the case when the THz absorption length $L_\alpha \equiv 1/\alpha_T$ (subscript T corresponds to THz) is much shorter than its diffraction length L_d, with $L_d \approx \pi n_T w_s^2/\lambda_T$. In this case, the THz field envelope E_T is determined to good accuracy by the local signal waves E_{s1} and E_{s2}, with $E_T(\mathbf{r}) \approx -2\pi i d_{\mathrm{eff},T} E_{s1}(\mathbf{r}) E_{s2}(\mathbf{r})^*/(n_T \lambda_T \alpha_T)$. Assuming this form of E_T and using coupled wave equations [9], the THz-OPA gain coefficient is given by

$$\left(\frac{g}{I_{s1}}\right)_{\text{THz-OPA}} = \frac{32\pi^2}{\epsilon_0 c n_{s1} n_{s2} n_T \lambda_{s2} \lambda_T} \frac{d_{\mathrm{eff},T}^2}{\alpha_T}, \qquad (2)$$

where for $LiNbO_3$, $d_{\mathrm{eff},T} \approx 97\,\mathrm{pm/V}$, $\alpha_T \approx 14.5\,\mathrm{cm}^{-1}$, $n_T \approx 5.2$, and $n_{s1} \approx n_{s2} \approx 2.13$ [14]. By substituting Eq. (2) into (1), $(G/P_{s1}) \approx 3.1 \times 10^{-2}\,\%/\mathrm{W}$; the corresponding THz-OPO threshold is 51 W. For our OPO, the resonating signal power at the THz-OPO threshold is approximately 77 W based on our loss estimates. Since the diffraction length $L_d \approx 414\,\mu\mathrm{m}$ (based on a $75\,\mu\mathrm{m}$ signal beam waist) is actually less than the absorption length $L_\alpha = \alpha_T^{-1} \approx 690\,\mu\mathrm{m}$, Eq. (2) slightly underestimates the THz-OPO threshold.

For the Raman process, the gain coefficient at the Stokes frequency for a $1.8\,\mu\mathrm{m}$ signal can be estimated as $(g/I_{s1}) \approx 2.52\,\mathrm{cm/GW}$ for the 18.92 THz Raman peak ($\approx 630\,\mathrm{cm}^{-1}$) [9]. From Eq. (1), this gain coefficient implies that $(G/P_{s1}) \approx 9.25 \times 10^{-3}\,\%/\mathrm{W}$, which is lower than the gain for the THz-OPA process. We observed Raman-shifted frequencies only when operating at pump powers above the THz-OPO threshold (i.e., when the OPO was no longer cw and single-mode), suggesting that a self-amplitude-modulation of the signal could have increased the SRS gain.

By increasing the losses at the cascaded-signal wavelengths, these processes can be avoided while still maintaining high pump depletion. This increase in loss could be achieved by increasing the cavity output coupling, or by using an intracavity etalon to introduce loss selectively at the cascaded-signal wavelengths [6]. For monolithic cavities, introducing an intracavity etalon is more challenging than for a ring-cavity OPO. However, for our OPO, approximately half of the THz-OPA gain occurred in the signal return-pass region of the cavity. Therefore, the THz-OPA gain could be halved by using a different poling period in this region, since a different THz frequency would then be phasematched instead; both THz waves would then see only half of the total gain. With this procedure, the THz-OPO could be suppressed at $N = 2.5$ without increasing the output coupling.

In conclusion, we have demonstrated a compact, tunable, and low-threshold source of narrow-linewidth radiation tunable between 1.75 and $1.95\,\mu\mathrm{m}$ based on a monolithic OPO in PPLN. We have identified cascaded Raman and THz generation as parasitic effects that can limit OPO performance, and shown quantitative agreement between experiments and theoretical predictions. Oscillation due to the THz-OPA process can be suppressed, at $N = 2.5$, by simultaneously scaling the OPO pump power and output coupling or by using a crystal with increased length or THz absorption. By understanding the processes we have discussed here and elsewhere [6], instabilities in OPOs can be avoided, thereby ensuring stable, compact, and single-frequency operation.

This research was supported by the U.S. Air Force Office of Scientific Research (USAFOSR) under grants FA9550-09-1-0233 and FA9550-05-1-0180.

References

1. S. T. Yang, R. C. Eckardt, and R. L. Byer, Opt. Lett. **18**, 971 (1993).
2. L. E. Myers and W. R. Bosenberg, IEEE J. Quantum Electron. **33**, 1663 (1997).
3. W. Kozlovsky, C. Nabors, R. Eckardt, and R. Byer, Opt. Lett. **14**, 66 (1989).
4. J. Pelc, C. R. Phillips, D. Chang, C. Langrock, and M. M. Fejer, Opt. Lett. **36**, 864 (2011).
5. M. Taya, M. C. Bashaw, and M. M. Fejer, Opt. Lett. **21**, 857 (1996).
6. C. R. Phillips and M. M. Fejer, J. Opt. Soc. Am. B **27**, 2687 (2010).
7. D. H. Jundt, Opt. Lett. **22**, 1553 (1997).
8. J. Kiessling, R. Sowade, I. Breunig, K. Buse, and V. Dierolf, Opt. Express **17**, 87 (2009).
9. R. Boyd, *Nonlinear Optics* (2008).
10. R. Sowade, I. Breunig, I. Cmara Mayorga, J. Kiessling, C. Tulea, V. Dierolf, and K. Buse, Opt. Express **17**, 22303 (2009).
11. A. V. Okishev and J. D. Zuegel, Opt. Express **14**, 12169 (2006).
12. A. Henderson and R. Stafford, Opt. Lett. **32**, 1281 (2007).
13. S. Schiller, "Principles and applications of optical monolithic total internal reflection resonators," Ph.D. thesis (Stanford University, 2006).
14. K. L. Vodopyanov, Laser Photon. Rev. **2**, 11 (2008).